Impacts of Coulomb Interactions on the Magnetic Responses of Excitonic Complexes in Single Semiconductor Nanostructures

**Wen-Hao Chang · Chia-Hsien Lin · Ying-Jhe Fu ·
Ta-Chun Lin · Hsuan Lin · Shuen-Jen Cheng ·
Sheng-Di Lin · Chien-Ping Lee**

Abstract We report on the diamagnetic responses of different exciton complexes in single InAs/GaAs self-assembled quantum dots (QDs) and quantum rings (QRs). For QDs, the imbalanced magnetic responses of inter-particle Coulomb interactions play a crucial role in the diamagnetic shifts of excitons (X), biexcitons (XX), and positive trions (X^-). For negative trions (X^-) in QDs, anomalous magnetic responses are observed, which cannot be described by the conventional quadratic energy shift with the magnetic field. The anomalous behavior is attributed to the apparent change in the electron wave function extent after photon emission due to the strong Coulomb attraction by the hole in its initial state. In QRs, the diamagnetic responses of X and XX also show different behaviors. Unlike QDs, the diamagnetic shift of XX in QRs is considerably larger than that of X. The inherent structural asymmetry combined with the inter-particle Coulomb interactions makes the wave function distribution of XX very different from that of X in QRs. Our results suggest that the phase coherence of XX in QRs may survive from the wave function localization due to the structural asymmetry or imperfections.

Keywords Quantum dots · Quantum rings · Magnetophotoluminescence · Diamagnetic shift

W.-H. Chang (✉) · C.-H. Lin · H. Lin · S.-J. Cheng
Department of Electrophysics, National Chiao Tung University,
Hsinchu 30010, Taiwan
e-mail: whchang@mail.nctu.edu.tw

Y.-J. Fu · T.-C. Lin · S.-D. Lin · C.-P. Lee
Department of Electronics Engineering, National Chiao Tung
University, Hsinchu 30010, Taiwan

Introduction

Single semiconductor nanostructures, such as quantum dots (QDs) and quantum rings (QRs), have attracted much attention due not only to their fundamental interest, but also to their potential applications in the prospective quantum information technology [1–8]. In semiconductor nanostructures, excitonic effects play a central role in their optical properties [9–15]. Electrons and holes form a variety of exciton complexes in QDs and QRs due to the enhanced Coulomb interactions by the spatial confinements. The spatial extents of excitonic wave functions thus reflect the both the combined effects of spatial confinements and the inter-particle Coulomb interactions among constituent charged carriers [9, 10, 13, 14]. Applying a magnetic field B is an efficient way to probe the spatial extent of excitonic wave functions. In a magnetic field B, the exciton emission energy increases quadratically with B, i.e., the diamagnetic shift $\Delta E = \gamma B^2$, with a diamagnetic coefficient γ proportional to the area of the excitonic wave function. Depending on the confinement regime of the nanostructures, the measured γ could have different physical meanings [9]. In the strong confinement regime, where the single-particle energy dominates over the Coulomb energies, γ is a measure of the spatial confinement of the QDs, while the magnetic responses of inter-particle Coulomb energies only appear as correction terms to the overall diamagnetism. On the other hand, when confined excitons are in the weak confinement regime, the Coulomb energies become prominent, such that γ will be mainly determined by the magnetic response of the inter-particle Coulomb interactions. For exciton complexes confined in nanostructures [14, 15], the diamagnetic behaviors are more complicated because of the more elaborate Coulomb interactions among the constituent charged carriers.

Therefore, a systematic investigation is essential into further understanding the magnetic responses of different exciton complexes in QDs or QRs.

In this work, we report on the diamagnetic response of different exciton complexes, including neutral excitons (X), biexcitons (XX), positive and negative trions (X^+ and X^-) confined in single InAs/GaAs self-assembled QDs and QRs. In QDs, the influences of imbalanced magnetic responses of Coulomb energies on the overall diamagnetisms of X, XX, and X^+ are observed and discussed. As for the magnetic response of X^- in QDs, we observe an anomalous diamagnetic behavior, which cannot be described by the conventional quadratic energy shift with the applied B. Such anomalous behaviors for X^- can be attributed to the apparent change in the electron wave function extent after photon emission due to the strong Coulomb attraction by the hole in its initial state. In QRs, the diamagnetic responses of X and XX also show different behavior. The impacts of inherent structural asymmetry of the self-assembled QRs, as well as the inter-particle Coulomb interactions, on the distribution of X and XX wave functions are discussed. Our results suggest that the phase coherence of XX in QRs may survive from the wave function localization due to the structural asymmetry or imperfections.

Experimental Details

The investigated samples were grown on GaAs (100) substrates by a molecular beam epitaxy system. For the QD sample, a layer of InAs self-assembled QDs (2.0 MLs) was grown on GaAs at 480°C without substrate rotations, yielding a gradient in area dot density ranging from 10^8 to 10^{10} cm^{-2}. Atomic force microscopy (AFM) of uncapped samples reveals that the dots are lens shaped, with an average height and diameter of $\approx 2(\pm 0.5)$ and ≈ 15 nm, respectively. The QDs were finally capped by a 100-nm undoped GaAs layer.

For the QR sample, a low-density InAs QD layer was first grown by depositing 2-ML InAs at 520°C as QR precursors. The substrate temperature was then lowered to 500°C for depositing a thin GaAs layer (1.7 nm) to cover the QD sidewalls, followed by a 50-s growth interruption for expelling the indium atoms from the QD center for the QR formation [16, 17]. Surface topography of uncapped QRs has also been investigated by AFM. The area density of surface QRs is about 10^7 cm^{-2}. Typical surface QRs have a rim diameter of 35 nm, a height of ≈ 1.3 nm, and a center dip of about 2 nm. The realistic dimension of the embedded QRs is expected to be much smaller [18]. We also found that the QR is anisotropic; the rim of the surface QR is higher along [$1\bar{1}0$].
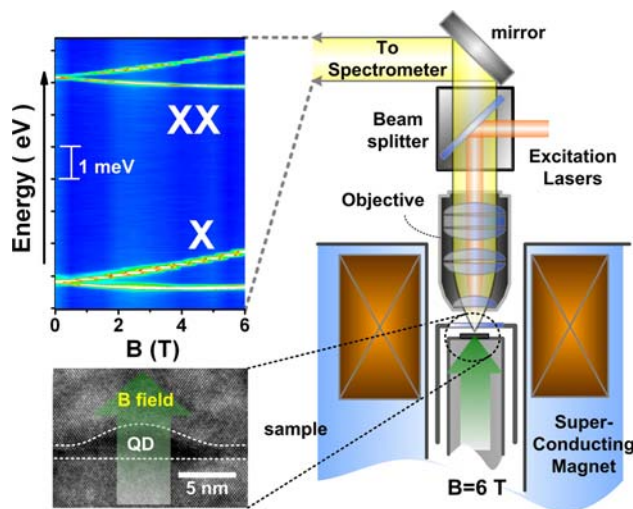

Fig. 1 Experimental setup for single-QD magneto-PL measurements

To isolate individual QDs or QRs for optical measurements, a 100-nm-thick Al metal mask was fabricated on the sample surface with arrays of 0.3-μm apertures using electron-beam lithography. Single QD spectroscopes were carried out at 5–8 K in a specially designed micro-photoluminescence (μ-PL) setup (see Fig. 1), where the sample was mounted in a low-temperature stage and inserted into the bore of 6-T superconducting magnet for magneto-PL measurements. A He–Ne laser beam or a cw Ti:Sapphire laser was focused onto the aperture through a microscope objective (NA = 0.5). The PL signals were collected by the same objective, analyzed by a 0.75-m grating monochromator, and detected by a liquid-nitrogen-cooled charged-coupled device (CCD) camera, which yield a resolution-limited spectral linewidth of about 60 μeV.

Results and Discussions

Quantum Dots

Several apertures containing only one QD have been investigated, and all of which showed similar spectral features. Typical single QD spectra consists of four dominant emission lines associated with the recombination of neutral excitons (X), biexcitons (XX), positive and negative trions (X^+ and X^-). These excitonic spectra have been unambiguously identified according to power-dependent and polarization-resolved PL measurements [14]. Magneto-PL measurements have been taken on a total of seven QDs with X energy distributed over the range of 1,349–1,385 meV. Typical spectra selected from one particular QD are shown in Fig. 2. When a magnetic field, B, was applied along the QD growth direction (Faraday geometry), each line splits into a doublet through the Zeeman effect. In
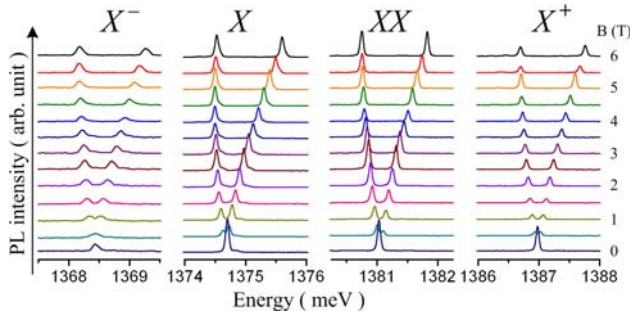
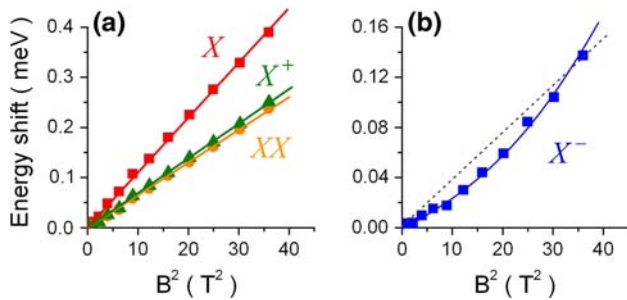**Fig. 2** Magneto-PL spectra for a typical QD measured under an applied B = 0–6 T

Fig. 3 a The energy shifts of X, X^+, and XX in a QD as a function of B^2. **b** The energy shifts of X^- as a function of B^2. A clear non-quadratic B dependence can be seen

addition, the average energy of each Zeeman doublet increases with the increasing B, known as the diamagnetic shift. In Fig. 3, the measured diamagnetic shifts for the four excitonic emission lines are plotted as a function of B^2. For X, X^+, and XX, the measured diamagnetic shifts show a quadratic dependence $\Delta E = \gamma B^2$, with a clear trend of $\gamma_X > \gamma_{XX} \cong \gamma_{X^+}$. This trend holds for all investigated dots and is a consequence of different magnetic responses of inter-particle Coulomb energies.

To explain this behavior, we consider here a 2D parabolic potential as the effective lateral confinement for both electrons and holes in the QDs, with a quantization energy of $\hbar\omega_\beta$ and a wave function extent of $\ell_\beta = \sqrt{\hbar/m_\beta\omega_\beta}$, where β denotes e or h and m_β are the effective masses [20, 21]. The use of parabolic model simplifies the problem considerably, because of the availability of analytical formula for all Coulomb interactions being parameterized by ℓ_β. The inter-particle direct Coulomb energy is given by [20–22]

$$V_{\alpha\beta} = \frac{e^2}{4\pi\varepsilon\varepsilon_0}\sqrt{\frac{\pi}{2}}\frac{1}{\ell}$$

where $\ell \equiv \sqrt{\left(\ell_\alpha^2 + \ell_\beta^2\right)/2}$. In a magnetic field B, ω_β can be replaced by the B-dependent hybridize frequency $\Omega_\beta(B) = \sqrt{\omega_\beta^2 + (eB/2m_\beta)^2}$. In the weak-field limit, the

B-dependent single-particle energy $\hbar\Omega_\beta(B)$ and the Coulomb energies $V_{\alpha\beta}(B)$ can be expanded analytically as,

$$\hbar\Omega_\beta(B) \approx \hbar\omega_\beta + \gamma_\beta^{\text{SP}}B^2 + \cdots \tag{1}$$

$$V_{\alpha\beta}(B) \approx V_{\alpha\beta}(0) + \gamma_{\alpha\beta}^{\text{Coul}}B^2 + \cdots \tag{2}$$

where $\gamma_\beta^{\text{SP}} = e^2\ell_\beta^2/8m_\beta$ is the single-particle diamagnetic coefficient, and $\gamma_{\alpha\beta}^{\text{Coul}} = k(\ell_\alpha^6 + \ell_\beta^6)/2\ell^3$ accounts for the magnetic response of $V_{\alpha\beta}(B)$, with a constant k defined as $\left(e^4\sqrt{\pi/2}/64\hbar^2\pi\varepsilon\varepsilon_0\right)$. If we take the Coulomb energies as perturbations to the single-particle energy in the strong confinement regime, the diamagnetic shift of X should be corrected as $\gamma_X = \left(\gamma_e^{\text{SP}} + \gamma_h^{\text{SP}}\right) - \gamma_{eh}^{\text{Coul}}$. On the other hand, the diamagnetic shift of XX will deviate from that of X by an amount of $\Delta\gamma = \gamma_X - \gamma_{XX} = 2\gamma_{eh}^{\text{Coul}} - \gamma_{ee}^{\text{Coul}} - \gamma_{hh}^{\text{Coul}}$. Because $\gamma_{\alpha\beta}^{\text{Coul}}$ varies as $\sim\ell^3$, a slight difference between ℓ_e and ℓ_h can lead to very different values for $\gamma_{ee}^{\text{Coul}}$, $\gamma_{eh}^{\text{Coul}}$ and $\gamma_{hh}^{\text{Coul}}$. Since $\ell_h < \ell_e$ and hence $\ell_h^3 \ll \ell_e^3$, we have $\gamma_{ee}^{\text{Coul}} \approx \gamma_{eh}^{\text{Coul}} \gg \gamma_{hh}^{\text{Coul}}$ that leads to $\Delta\gamma = \gamma_X - \gamma_{XX} \approx \gamma_{ee}^{\text{Coul}}$. The same arguments can be applied to the X^+ case, where γ_{X^+} is also reduced by a similar amount, in agreement with our experimental observations. The reason for $\gamma_{X^+} \approx \gamma_{XX}$ can also be understood from the fact that the emission energies of XX and X^+ are usually correlated even in different QDs [23], because their energy difference $E_{XX} - E_{X^+}$ equals roughly to $V_{ee} - V_{eh}$, which is value less sensitive to the magnetic field.

It is worth to emphasize that the systematic differences among γ_X, γ_{XX}, and γ_{X^+} could be observed only when ℓ_e and ℓ_h exhibit a large difference. For small InAs QDs, electron gradually lose confinement as the dot size reduces, which in turn push the electron level toward the wetting-layer continuum, resulting in a more extended electron wave function penetrating into the barrier material [24]. On the other hand, the hole wave function remains well localized in the QDs, leading to a large difference between ℓ_e and ℓ_h. For larger In(Ga) As QDs, since ℓ_e and ℓ_h are expected to be similar, the diamagnetic response of all exciton complexes will be nearly identical [13], so that the magnetic response of interparticle Coulomb energies of such strongly confined few-particle systems becomes unable to resolve experimentally.

For the case of X^- in QDs, its magnetic response shows an anomalous behavior, which does not follow the conventional B^2-dependence energy shift, as can be seen from Fig. 3b. Our measurements show that the X^- diamagnetic shifts in most QDs investigated are smaller and non-quadratic. To understand the peculiar behavior, the charge configurations of the initial and the final states of X^- should be considered. As depicted in Fig. 4, the initial state of X^- consists of two electrons and one hole, which will
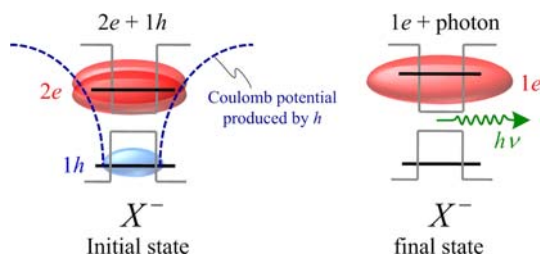
Fig. 4 A schematic for the charge configurations of X^- in QDs before and after photon emissions. The final-state electron is more extended due the Coulomb attraction of the hole in its initial state

leave one electron in its final state after recombination. The X^- diamagnetic shift thus reflects the diamagnetic responses of both the initial and final states. We have performed numerical model simulations using single-band Hamiltonian of cone-shape QDs including Hartree approximations to calculate the lateral extents of the initial-state $\ell_{e,i}$ and the final-state $\ell_{e,f}$ electron wave functions of X^-. We found that the $\ell_{e,f}$ is always more extended than $\ell_{e,i}$. This can be realized from the presence of hole in its initial state, which contracts the electron wave function by the Coulomb attraction. As the QD sizes reduces, $\ell_{e,f}$ increases rapidly, due to the penetration of electron wave function into the barrier material [24]. The very extended electron becomes sensitive to the long-range Coulomb attractive potential produced by the hole in the initial state, by which $\ell_{e,i}$ will be contracted and become apparently smaller than $\ell_{e,f}$. As a result, the final-state diamagnetic shift increases, so that the overall diamagnetic shift in X^- is reduced. This phenomenon is not expected for X^+ in QDs, since the wave function extents of the initial- and final-state holes are almost identical due to the fact that hole has a larger effective mass, such that the hole wave function remains well confined even in small QDs. Therefore, the Coulomb attractive potential produced by the weakly confined electron becomes less important.

Now, we explain why the X^- diamagnetic shift exhibits a non-quadratic B dependence. To illustrate this behavior, we consider the diamagnetic shift in the carrier's single-particle energy and expand it in powers of B as, $\hbar\Omega_\beta(B) = \hbar\omega_\beta + \gamma_\beta^{SP}B^2 + \kappa_\beta^{SP}B^4 + \cdots$, where the quartic coefficient κ_β^{SP} is negative and is given by $\kappa_\beta^{SP} = -e^4\ell_\beta^6/128m_\beta\hbar^2$. By taking into account the difference between $\ell_{e,i}$ and $\ell_{e,f}$, a simple algebraic analysis for the X^- diamagnetic shift, $\Delta E_{X^-}(B)$, gives the following expression:

$$\Delta E_{X^-}(B) \approx \gamma_{X^-}B^2 + \kappa_{X^-}B^4 + \cdots, \tag{3}$$

where $\gamma_{X^-} = \left(2\gamma_{e,i}^{SP} + \gamma_{h,i}^{SP}\right) - \gamma_{e,f}^{SP}$ and $\kappa_{X^-} = \left(2\kappa_{e,i}^{SP} + \kappa_{h,i}^{SP}\right) - \kappa_{e,f}^{SP}$. Because of $\ell_h < \ell_e$ and $m_h \gg m_e$, $\gamma_{h,i}^{SP}$ and $\kappa_{h,i}^{SP}$ only have minor influences on the overall diamagnetism. Accordingly, we obtain $\gamma_{X^-} \approx 2\gamma_{e,i}^{SP} - \gamma_{e,f}^{SP} =$

$e^2\left(2\ell_{e,i}^2 - \ell_{e,f}^2\right)/8m_e$ and $\kappa_{X^-} \approx 2\kappa_{e,i}^{SP} - \kappa_{e,f}^{SP} = -e^2\left(2\ell_{e,i}^6 - \ell_{e,f}^6\right)/128m_e\hbar^2$. Equation (3) makes clear how the difference in $\ell_{e,i}$ and $\ell_{e,f}$ can lead to anomalous diamagnetic shifts for X^-. For a normal case of $\ell_{e,i} \approx \ell_{e,f} = \ell_e$, we have $\gamma_{X^-} \approx \gamma_e \approx \gamma_X$ and $\gamma_{X^-} \gg \kappa_{X^-}$. That is, the X^- diamagnetic shift behaves as the usual B^2 dependence with a coefficient similar to that of X. A very interesting case occurs when $\sqrt{2}\ell_{e,i} = \ell_{e,f}$, which leads to $2\gamma_{e,i} = \gamma_{e,f}$ and cancels out the B^2 term, resulting in a dominant B^4-dependent energy shift. The energy shift shown in Fig. 3(b) exhibits both quadratic and quartic B dependence. Therefore, the measured curvature can also be a sensitive probe to the change in wave function extents between the initial and the final-state electrons of X^-.

Quantum Rings

Figure 5a and b show the surface topography and line scans along [110] and [1$\bar{1}$0] directions of uncapped QRs. Typical single-QR magneto-PL spectra are shown in Fig. 5c. Two emission lines associated with the recombination from X and XX can be observed. The same measurement has been performed on a total of seven QRs with X emission energies ranging from 1,320 to 1,328 meV. Apart from the Zeeman splitting, both X and XX show clear diamagnetic shifts with the increasing B. The average diamagnetic coefficient of X
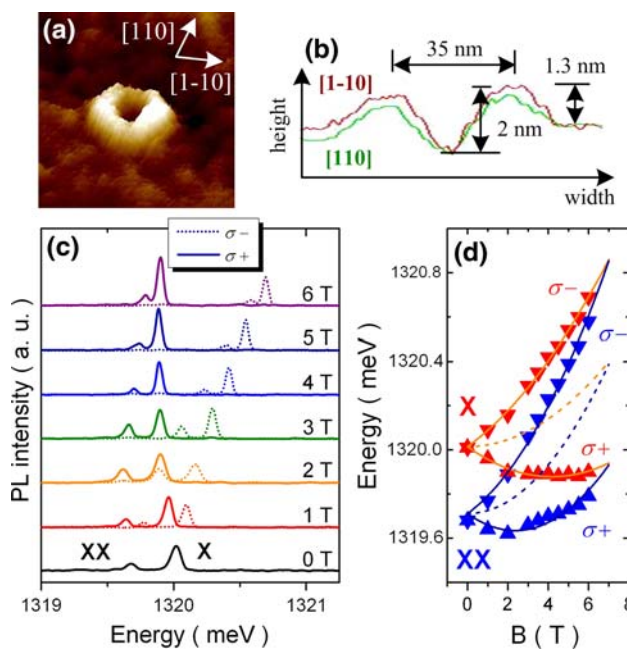

Fig. 5 a Surface topography and **b** line scans along [110] and [1$\bar{1}$0] directions of uncapped QRs. **c** Typical single-QR magneto-PL spectra taken under different applied B. **d** The B-dependent energy shifts of the X and XX. *Solid* and *dashed lines* are fitting curves using quadratic B dependence

for all the investigated QRs is $\gamma_X = 6.8\,\mu eV/T^2$. Interestingly, we found that XX shows a considerably larger diamagnetic coefficient with an average value of $\gamma_{XX} = 14.8\,\mu eV/T^2$, which is more than the double of the γ_X value.

The larger γ_{XX} indicates a more extended XX wave function in QRs. This is different from the case of QDs, where γ_{XX} is usually similar to, or somewhat smaller than, γ_X due to the different spatial extents of the electron and hole wave functions and their responses to the applied B. Here, we argue that the larger γ_{XX} is a consequence of the fact that self-assembled QRs do not have perfect azimuthal symmetry. It has been reported that buried self-assembled QRs exhibit an asymmetric craterlike shape, with a diameter substantially smaller than the ring-shaped islands on the surface of uncapped QR structures [18]. In addition, due to the preferential out diffusion of dot material along the [1$\bar{1}$0] direction, the embedded rim height is higher along the [110] direction, resulting in two separate potential valleys along the [110] direction, resembling a pair of connected QDs [19]. Based on the proposed shape for embedded QRs in Ref. [19], we have performed theoretical calculations for the wave function distributions of X and XX in QRs, which are shown in Fig. 6. Although the actual shape of embedded QRs is not known exactly, the numerical model used here is still a good illustration when QRs have any structural imperfection. Using selective chemical etching to remove the GaAs capping layer may be an efficient way to reveal the structure of buried QRs [25, 26].
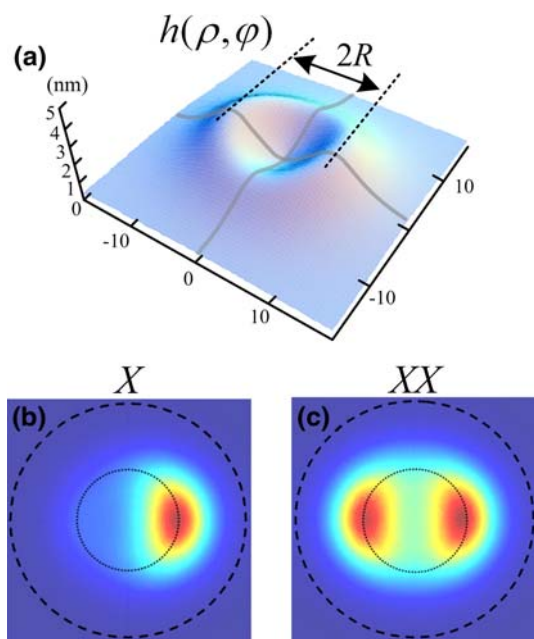

Fig. 6 a A schematic for the QR geometry with a structural anisotropy used in model calculations. **b** and **c** are the calculated electron wave functions of the lowest X and XX states. The *dash circle* represents the rim diameter of 14 nm

The lack of rotational symmetry in the potential of embedded QRs has significant impacts on the diamagnetic responses of X and XX. For X confined in QRs, the height variation strongly localizes the hole in one of the potential valleys due to the large effective mass. Consequently, the electron will be bound to the same valley by the electron–hole Coulomb attraction. This means that the wave function extent of X is determined mainly by the confinement of the potential valley and the Coulomb interaction. Therefore, the diamagnetic response of X is similar to an elliptic QD.

For XX confined in QRs, the two holes may be separately localized in different valleys due to the strong hole–hole Coulomb repulsion. Due to the Coulomb attractions of the two separately localized holes, the electron wave functions of XX are more likely to spread over the two valleys and become more extended than that of X. Unlike X, the wave function extent of XX is determined mainly by the diameter of the embedded QRs. This explains why γ_{XX} is significantly larger than γ_X for QRs.

Before conclusions, we would like to comment on the implications of the larger diamagnetic shift of XX in QRs. Charged particles confined to a QR are expected to show the well-known Aharanov–Bohm (AB) effect due to the quantum interference of the carrier's wave function in the ring-shaped geometry [6–8]. However, for an exciton confined in ring-like nanostructures, the AB effect is not expected to occur for such a charge-neutral composite unless the electron and hole can propagate coherently in different trajectories with a non-zero electric dipole moment [27]. This can occur naturally in type-II QD systems, where the electron and hole are spatially separated [28, 29]. However, for InGaAs self-assembled QRs where both the electron and hole are confined, it is still an open question whether the excitonic AB effect can be observed. In fact, this issue is further complicated by the inherent structural asymmetry and/or imperfections presented inevitably in self-assembled QRs [18, 19]. Our results suggest that the inherent structural asymmetry combined with the inter-particle Coulomb interactions tends to localize the X wave function and hence may smear out its phase coherence. On the other hand, due to hole–hole repulsion, the XX wave function is more extended and spread over the entire ring. Therefore, the phase coherence of XX may be more likely to survive from such wave function localizations at lower magnetic field.

Conclusions

In conclusion, the diamagnetic response of different exciton complexes, including neutral excitons (X), biexcitons (XX), positive and negative trions (X^+ and X^-) confined in single InAs/GaAs self-assembled QDs and QRs has been

investigated. In QDs, we found a systematic trend of $\gamma_X > \gamma_{XX} \approx \gamma_{X+}$ caused by the imbalanced magnetic responses of inter-particle Coulomb interactions, which could be observed only when the confined electron and hole wave functions exhibit a large difference in their lateral extents. Furthermore, the difference $\Delta\gamma = \gamma_X - \gamma_{XX}$ was found to scale as the cube of its single-particle wave function extent and therefore can be a sensitive probe to the electron-hole wave function asymmetry. On the other hand, the magnetic response of X^- in QDs fell into a special regime where the conventional quadratic diamagnetic shift failed to describe its magnetic response. Our measurements show that the X^- diamagnetic shifts in most QDs investigated are even smaller and non-quadratic. Such anomalous behaviors for X^- were explained by the apparent change in the electron wave function extent after photon emission due to the strong Coulomb attraction induced by the hole in its initial state. In QRs, the diamagnetic responses of X and XX also show different behavior. Unlike single QDs, XX in QRs shows a considerably larger diamagnetic coefficient than the X. Numerical model calculations indicate that the inherent structural asymmetry and imperfection of the self-assembled QRs, combined with the inter-particle Coulomb interactions, play a crucial role in the distribution of X and XX wave functions. Our results suggest that the phase coherence of XX in QRs may survive from the wave function localization due to the structural asymmetry or imperfections.

References

1. P. Michler, A. Kiraz, C. Becher, W.V. Schoenfeld, P.M. Petroff, L. Zhang, E. Hu, A. Imamoglu, Science **290**, 2282 (2000)
2. M. Pelton, C. Santori, J. Vuckovic, B. Zhang, G.S. Solomon, J. Plant, Y. Yamamoto, Phys. Rev. Lett. **89**, 233602 (2002)
3. Z. Yuan, B.E. Kardynal, R.M. Stevenson, A.J. Shields, C.J. Lobo, K. Cooper, N.S. Beattie, D.A. Ritchie, M. Pepper, Science **295**, 102 (2002)
4. W.-H. Chang, W.-Y. Chen, H.-S. Chang, T.-P. Hsieh, J.-I. Chyi, T.-M. Hsu, Phys. Rev. Lett. **96**, 117401 (2006)
5. X. Li, Y. Wu, D. Steel, D. Gammon, T.H. Stievater, D.S. Katzer, D. Park, C. Piermarocchi, L.J. Sham, Science **301**, 809 (2003)
6. A. Lorke, R.J. Luyken, A.O. Govorov, J.P. Kotthaus, J.M. García, P.M. Petroff, Phys. Rev. Lett. **84**, 2223 (2000)
7. M. Bayer, M. Korkusinski, P. Hawrylak, T. Gutbrod, M. Michel, A. Forchel, Phys. Rev. Lett. **90**, 186801 (2003)
8. N.A.J.M. Kleemans, I.M.A. Bominaar-Silkens, V.M. Fomin, V.N. Gladilin, D. Granados, A.G. Taboada, J.M. García, P. Offermans, U. Zeitler, P.C.M. Christianen, J.C. Maan, J.T. Devreese, P.M. Koenraad, Phys. Rev. Lett. **99**, 146808 (2007)
9. S.N. Walck, T.L. Reinecke, Phys. Rev. B **57**, 9088 (1998)
10. M. Bayer, S.N. Walck, T.L. Reinecke, A. Forchel, Phys. Rev. B **57**, 6584 (1998)
11. Y. Naganume, Y. Arakawa, S. Tsukamoto, M. Nishioka, S. Sasaki, N. Miura, Phys. Rev. Lett. **69**, 2963 (1992)
12. T. Someya, H. Akiyama, H. Sakaki, Phys. Rev. Lett. **74**, 3664 (1995)
13. C. Schulhauser, D. Haft, R.J. Warburton, K. Karrai, A.O. Govorov, A.V. Kalameitsev, A. Chaplik, W. Schoenfeld, J.M. Garcia, P.M. Petroff, Phys. Rev. B **66**, 193303 (2002)
14. M.-F. Tsai, H. Lin, C.-H. Lin, S.-D. Lin, S.-Y. Wang, M.-C. Lo, S.-J. Cheng, M.-C. Lee, W.-H. Chang, Phys. Rev. Lett. **101**, 267402 (2008)
15. T.-C. Lin, C.-H. Lin, H.-S. Ling, Y.-J. Fu, W.-H. Chang, S.-D. Lin, C.-P. Lee, Phys. Rev. B **80**, 081304(R) (2009)
16. D. Granados, J.M. García, Appl. Phys. Lett. **82**, 2401 (2003)
17. H.S. Ling, C.P. Lee, J. Appl. Phys. **102**, 024314 (2007)
18. P. Offermans, P.M. Koenraad, J.H. Wolter, D. Granados, J.M. García, V.M. Fomin, V.N. Gladilin, J.T. Devreese, Appl. Phys. Lett. **87**, 131902 (2005)
19. V.M. Fomin, V.N. Gladilin, S.N. Klimin, J.T. Devreese, N.A.J.M. Kleemans, P.M. Koenraad, Phys. Rev. B **76**, 235320 (2007)
20. S.-J. Cheng, W. Sheng, P. Hawrylak, Phys. Rev. B **68**, 235330 (2003)
21. S.-J. Cheng, Phys. Rev. B **76**, 075329 (2007)
22. R.J. Warburton et al., Phys. Rev. B **58**, 16221 (1998)
23. S. Rodt, A. Schliwa, K. Pötschke, F. Guffarth, D. Bimberg, Phys. Rev. B **71**, 155325 (2005)
24. K.L. Janssens, F.M. Peeters, V.A. Schweigert, Phys. Rev. B **63**, 205311 (2001)
25. Z.M. Wang, L. Zhang, K. Holmes, G.J. Salamo, Appl. Phys. Lett. **86**, 143106 (2005)
26. F. Ding, L. Wang, S. Kiravittaya, E. Müller, A. Rastelli, O.G. Schmidt, Appl. Phys. Lett. **90**, 173104 (2007)
27. A.O. Govorov, S.E. Ulloa, K. Karrai, R.J. Warburton, Phys. Rev. B **66**, 081309R (2002)
28. E. Ribeiro, A.O. Govorov, W. Carvalho Jr, G. Medeiros-Ribeiro, Phys. Rev. Lett. **92**, 126402 (2004)
29. I.R. Sellers, V.R. Whiteside, I.L. Kuskovsky, A.O. Govorov, B.D. McCombe, Phys. Rev. Lett. **100**, 136405 (2008)